

# DNANet: De-Normalized Attention Based Multi-Resolution Network for Human Pose Estimation

Kun Zhang<sup>1,2\*</sup>, Peng He<sup>1,2\*</sup>, Ping Yao<sup>1,2\*</sup>, Ge Chen<sup>1,2</sup>, Chuanguang Yang,  
Huimin Li<sup>3</sup>, Li Fu<sup>1,2</sup>, Tianyao Zheng<sup>1,2</sup>

<sup>1</sup>School of Computer Science and Technology, University of Chinese Academy of Sciences,

<sup>2</sup>Institute of Computing Technology, Chinese Academy of Sciences, <sup>3</sup>School of Automation, Beijing Institute of Technology

## Abstract

Recently, multi-resolution networks (such as Hourglass, CPN, HRNet, etc.) have achieved significant performance on the task of human pose estimation by combining features from various resolutions. In this paper, we propose a novel type of attention module, namely De-Normalized Attention (DNA) to deal with the feature attenuations of conventional attention modules. Our method extends the original HRNet with spatial, channel-wise and resolution-wise DNAs, which aims at evaluating the importance of features from different locations, channels and resolutions to enhance the network capability for feature representation. We also propose to add fine-to-coarse connections across high-to-low resolutions inside each layer of HRNet to increase the maximum depth of network topology. In addition, we propose to modify the keypoint regressor at the end of HRNet for accurate keypoint heatmap prediction.

Our proposed network for keypoint estimation have achieved state-of-the-art performance at 77.9 AP score on COCO val2017 dataset and 77.0 on COCO test-dev dataset without using extra keypoint training data. Our paper will be accompanied with publicly available codes at GitHub.

## 1. Introduction

2D human pose estimation refers to the task of providing accurate pixel-level locations for human keypoints (such as head, shoulders, knees, ankles, etc.) from digital images, which remains an important but challenging problem in the field of computer vision. This paper is related to single person pose estimation, which remains an active research topic for decades and serves as basic technology to solve several practical applications such as pose tracking (Iqbal, Milan, and Gall 2017; Insafutdinov et al. 2017; Xiao, Wu, and Wei 2018; Xiu et al. 2018), human action recognition (Xu et al. 2015; Kar et al. 2017; Zhou et al. 2018; Zhang et al. 2018), human computer interaction (Xu et al. 2017; Yan,

Xiong and Lin 2018), etc. In recent years, the progress on the task of human pose estimation has been significantly benefited by the rich representation power of convolution neural networks (Toshev and Szegedy 2014; Wei et al. 2016; Carreira et al. 2016).

Accurate keypoint estimation networks need not only low-level features with high resolutions for precise keypoint prediction, but also high-level features with large receptive fields for invisible keypoint inference. State of the art methods on pose estimation tend to fuse multi-resolution features to satisfy these two requirements. For instance, Hourglass-based networks (Newell, Yang, and Deng 2016; Ke et al. 2018; Yang et al. 2017) capture and consolidate features across various scales by repeating symmetric network structures; Pyramid-based networks (Chen et al. 2018; Su et al. 2019) integrate information from different ResNet stages via GlobalNet and RefineNet; HRNet (Sun et al. 2019) keeps high resolution representations through the network and fuses multi-scale features in each stage to enrich feature representations. These networks have achieved significant results on human pose estimation by fusing features from different resolutions.

Recently, attention models (Vaswani et al. 2017; Shen et al. 2018) have obtained promising performance in the field of computer vision with emerging and increasing applications, such as image classification (Wang et al. 2017; Hu, Shen, and Sun 2018; Woo et al. 2018; Li, Hu, and Yang 2019), object detection (Dong et al. 2017; Zhu et al. 2019), image generation (Ma et al. 2018; Mejjati et al. 2018; Zhang et al. 2019), and semantic segmentation (Yu et al. 2018; Li et al. 2018; Fu et al. 2019). Attention modules usually generate normalized weights with Sigmoid or SoftMax functions for feature aggregation. However, with all weights generated by normalized functions constantly less than 1, multiplying features with normalized weights attenuates all features, which is especially noticeable in multi-attention systems (Woo et al. 2018; Fu et al. 2019; Su et al. 2019).

---

\*These authors contribute equally to the work.

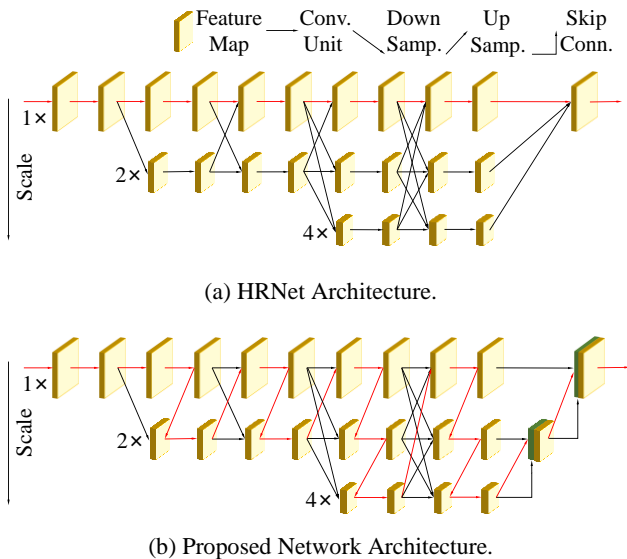


Figure 1: Comparing architecture of HRNet with our proposed network. (a) presents the architecture of HRNet, which consists of parallel multi-resolution sub-networks with information fusion between stages. (b) indicates the architecture of our proposed network with fine-to-coarse connections inside stages and final regression modification. The red arrows denote the longest path of network topologies. The length of longest paths for HRNet and our proposed network are 12 and 25 respectively in this figure.

To address this disadvantage of attentions, we present a novel type of attention module, namely De-Normalized Attention (DNA), applying affine transformation as de-normalizing operation to rescale normalized weights, so that they're no longer limited in the range of (0, 1). Similar to CSARB (Su et al. 2019), we extend HRNet with spatial and channel-wise De-Normalized Attentions, and we also newly introduce resolution-wise De-Normalized Attention to enhance feature fusion. With the help of three attentions, our proposed network is able to evaluate the importance of features from different locations, channels, and resolutions for precise human keypoint estimation. The three attention modules are illustrated in Figures 2, 3, 5 respectively.

As is shown in Figure 1(a), HRNet consists of parallel multi-resolution sub-networks with information fusion between stages, but we believe that information exchange across resolutions in each stage of network is also valuable. From this point of view, we propose to add fine-to-coarse connections across different resolutions inside each layer of HRNet, which extends the longest path of the network topology. Longest path represents the depth of neural network, and deepening network is generally considered to be able to enhance the capability for feature representations. In addition, we also propose to modify the final regressor of HRNet with deconvolutions, concatenations and skip connections for accurate keypoint estimation. Our network architecture is presented in Figure 1(b).

We empirically show the performance of proposed network on COCO keypoint detection dataset (Lin et al. 2014). Additionally, ablation studies indicate the effectiveness of our proposed modules. Our main contributions are three-fold as follows:

- We newly introduce De-Normalized Attentions (DNAs), applying affine transformations to deal with attenuations in attention modules. Also, we extend HRNet with three DNA modules to evaluate feature importance.
- We modify the architecture of HRNet in two ways. We add fine-to-coarse connections in each layer of HRNet to lengthen the longest path of network topology, and we alter keypoint regressor at the end of HRNet with skip connections, deconvolutions, and concatenations.
- We have achieved state-of-the-art performance on COCO benchmark without using extra keypoint training data.

## 2. Related Work

### 2.1 Attention Mechanism

Attention modules were broadly applied for modeling long-term dependencies in practical applications. They were initially developed for image classification (Mnih et al. 2014), but became popular for promising performance on natural language processing tasks such as machine translation (Bahdanau, Cho, and Bengio 2015; Vaswani et al. 2017), text summary (Rush, Chopra, and Weston 2015; Duan et al. 2019), and reading comprehension (Cui et al. 2016; Chen et al. 2019).

In recent years, attention modules were also increasingly used for computer vision tasks such as image classification (Wang et al. 2017; Hu, Shen, and Sun 2018; Woo et al. 2018; Li, Hu, and Yang 2019), image generation (Ma et al. 2018; Mejjati et al. 2018; Zhang et al. 2019), semantic segmentation (Yu et al. 2018; Li et al. 2018; Fu et al. 2019), and object detection (Dong et al. 2017; Zhu et al. 2019). Different from previous work, we propose to apply affine transformations as de-normalizing operations to rescale normalized weights in attention modules to tackle with feature attenuation of conventional attentions.

### 2.2 Multi-Resolution Networks

High-resolution features are beneficial to provide accurate pixel-level locations, while low-resolution features are able to represent global contexts for inference. Taking these two facts into account, features of high and low resolutions are both of importance in pixel labeling tasks. For instance, human pose estimation (Sun et al. 2019; Newell, Yang, and Deng 2016; Chen et al. 2018), semantic segmentation (Ronneberger, Fischer, and Brox 2015; Badrinarayanan, Kendall, and Cipolla 2017), and facial landmark detection (Lv et al. 2017; Xiao et al. 2016).

There are two mainstreams of multi-resolution networks: one mainstream is recovering high-resolution features from low-resolution representations generated by downsampling process (Noh, Hong, and Han 2015; Newell, Yang, and Deng 2016; Yang et al. 2017; Lin et al. 2017); the other is maintaining high resolution representations across the whole progress in neural networks (Saxena and Verbeek 2016; Zhou, Hu, and Zhang 2015; Fourure et al. 2017; Sun et al. 2019). Our approach follows the second mainstream, which extends modified HRNet with three DNA modules.

### 2.3 Human Pose Estimation

Human pose estimation remains an active topic for decades. Conventional approaches formulate this problem as graph models (Kiefel and Gehler 2014; Hara and Chellappa 2013), tree models (Wang and Mori 2008; Fu, Zhang, and Huang 2015), or forest models (Sun, Kohli, and Shotton 2012; Dantone et al. 2013), which are usually combined with handcraft features for keypoint predictions.

Recently, human pose estimation has been significantly benefited by the representation capability of convolutional neural networks (CNNs). Previous CNN based approaches for human pose estimation are mainly divided into three groups. Early representative works (Toshev and Szegedy 2014; Wei et al. 2016; Carreira et al. 2016) calculate joint locations with multi-stage regressions. Apart from that, some studies (Dong et al. 2014; Nie et al. 2018; Liang et al. 2019) consider human parsing and human pose estimation as multi-task problems, and carry them out simultaneously. In addition, similar to semantic segmentation, recent pose estimation methods (Newell, Yang, and Deng 2016; Chen et al. 2018; Sun et al. 2019) represent joint positions with Gaussian peaks and estimate keypoint heatmaps for pixel-level locations. Our approach follows the last method.

## 3. Method

We adopt High-Resolution Network (HRNet) as the basic network, on which we test the effectiveness of proposed methods. In this section, we firstly review the structure of HRNet briefly and then elaborate our proposed approaches.

### 3.1 Revisiting High Resolution Network

Given an image  $\mathbf{I}$  of size  $W \times H \times 3$ , the goal of HRNet (Sun et al. 2019) is to predict heatmap of size  $W' \times H' \times K$ , which indicates the location confidence of  $K$  joints. HRNet consists of three parts: a stem with strided convolutions to decrease resolution, a main body for feature extraction, and a final regressor for heatmap estimation.

As is shown in Figure 1(a), the main body of HRNet starts from a subnetwork of high resolution at the first stage, and gradually adds low-resolution subnetworks in following stages. Similar to Residual Networks (He et al.

2016), the subnetworks in stages of HRNet are composed of sequential residual units. Assuming that  $s$  is stage index and  $r$  is resolution index,  $N_{sr}$  denotes the subnetwork in the  $s$ th stage and the  $r$ th resolution (the  $r$ th resolution is  $1/2^{r-1}$  of the first resolution). An example of main body with four resolutions is illustrated as follows,

$$\begin{array}{ccccccc} N_{11} & \rightarrow & N_{21} & \rightarrow & N_{31} & \rightarrow & N_{41} \\ & & \searrow & & N_{22} & \rightarrow & N_{32} & \rightarrow & N_{42} \\ & & & & \searrow & & N_{33} & \rightarrow & N_{43} \\ & & & & & & \searrow & & N_{44} \end{array} \quad (1)$$

Repeated information fusion modules are applied inside and between stages for feature aggregation. Suppose stage  $s$  contains feature maps across  $M$  resolutions, the inputs of fusion module are  $\mathbf{X} = \{\mathbf{X}_1, \mathbf{X}_2, \dots, \mathbf{X}_M\}$ , and the outputs are  $\mathbf{Y} = \{\mathbf{Y}_1, \mathbf{Y}_2, \dots, \mathbf{Y}_M\}$ , in which  $\mathbf{Y}_i = \sum_{i=1}^M T(\mathbf{X}_h, i)$ . Function  $T(\mathbf{Y}_h, i)$  represents upsampling or downsampling operation from the  $i$ th resolution to the  $h$ th resolution. By combining parallel subnetworks and fusion modules, HRNet have achieved significant performance on pose estimation.

### 3.2 DNAs: De-Normalized Attentions

Attention module usually transforms encoded feature map  $\mathbf{E}$  with Sigmoid or SoftMax function to obtain weight  $\mathbf{W}$  for feature multiplication, i.e.,

$$\begin{array}{l} \mathbf{W} = \text{Sigmoid}(\mathbf{E}) \\ \text{or } \mathbf{W} = \text{SoftMax}(\mathbf{E}). \end{array} \quad (2)$$

Since the range of Sigmoid and SoftMax functions are both  $(0, 1)$ , it's obvious that absolute values of elements in feature map  $\mathbf{F}$  become smaller after multiplication with normalized weight  $\mathbf{W}$ . In other words, the intensities of features are attenuated, which are especially noticeable in multi-attention systems.

To address this shortcoming, we propose a novel type of attention module, namely De-Normalized Attention (DNA), applying affine transformation as de-normalizing operation with weight  $\omega$  and bias  $b$  to rescale normalized attentions, so that they're no longer limited in the range of  $(0, 1)$ . The De-Normalized Attention weights  $\mathbf{W}'$  are computed as:

$$\begin{array}{l} \mathbf{W}' = \text{Affine}(\text{Sigmoid}(\mathbf{E})) \\ \text{or } \mathbf{W}' = \omega(\text{SoftMax}(\mathbf{E})) + b. \end{array} \quad (3)$$

We extend residual units with spatial and channel-wise De-Normalized Attentions to enhance features in spatial and channel contexts, which is similar to CSARB (Su et al. 2019). Additionally, we newly introduce resolution-wise De-Normalized Attention for efficient information fusion between stages. The following parts of this subsection will describe details of these attention modules respectively.

### 3.2.1 cDNA: Channel-wise De-Normalized Attention

Channel-wise features in pose estimation can be regarded as responses for joints under specific backgrounds. Our Channel-wise De-Normalized Attention module calculates channel-wise weights by modelling relationship between responses. Following Squeeze-and-Excitation Net (Hu, Shen, and Sun 2018), our channel-wise attention contains two steps: squeezing step and excitation step respectively.

In squeezing step, we firstly aggregate input feature map  $\mathbf{F}_{ch}$  of size  $W \times H \times C$  with average-pooling and max-pooling functions to generate contextual descriptors of size  $1 \times 1 \times C$ , which is similar to CBAM (Woo et al. 2018). Then both descriptors are forwarded to fully connected layers  $\text{FC}_1$  and  $\text{FC}_2$  to reduce their dimensions to  $1 \times 1 \times S$ . Finally, we merge reduced features  $\mathbf{E}_{ch1}$  and  $\mathbf{E}_{ch2}$  with concatenation to get squeezed feature of size  $1 \times 1 \times 2S$ . In short, the squeezing step is computed as:

$$\mathbf{E}_{ch1} = \text{FC}_1(\text{AvgPool}(\mathbf{F}_{ch})), \quad (4)$$

$$\mathbf{E}_{ch2} = \text{FC}_2(\text{MaxPool}(\mathbf{F}_{ch})), \quad (5)$$

$$\mathbf{E}_{ch} = \text{Concat}(\mathbf{E}_{ch1}, \mathbf{E}_{ch2}). \quad (6)$$

In excitation step, we firstly use a simple gating function with Sigmoid and fully connected layer  $\text{FC}_3$  to extend squeezed feature  $\mathbf{E}_1$ . Then we apply affine transformation with weight  $\omega_{ch}$  and bias  $b_{ch}$  to rescale activated attentions. The excitation step of our cDNA module is computed as:

$$\mathbf{W}_{ch}' = \omega_{ch}(\text{Sigmoid}(\text{FC}_3(\mathbf{E}_{ch}))) + b_{ch}. \quad (7)$$

After squeezing and excitation steps, we multiply our learned channel-wise attention weights with input feature map to enhance useful responses, i.e.,

$$\mathbf{F}_{ch}' = \mathbf{W}_{ch}' \otimes \mathbf{F}_{ch}, \quad (8)$$

where  $\otimes$  denotes element-wise multiplication, and  $\mathbf{F}_{ch}'$  is feature enhanced by cDNA module. Detailed operations for channel-wise DNA are demonstrated in Figure 2.

### 3.2.2 sDNA: Spatial De-Normalized Attention

Spatial attention modules attempt to highlight useful local features for accurate keypoint prediction by adaptively encoding contextual information into local features, which are considered complementary to channel-wise attention modules. Our Spatial DNA module (sDNA) is similar to other spatial attentions but rescales attention weight with de-normalizing function. The schema of our sDNA module is illustrated in Figure 3.

Suppose  $\mathbf{F}_{st}$  is input feature map of size  $W \times H \times C$  for spatial attention, we firstly apply  $1 \times 1$  convolution, max-pooling and average-pooling functions along the channel axis simultaneously to generate various feature maps, which are denoted as  $\mathbf{E}_{st1}$ ,  $\mathbf{E}_{st2}$  and  $\mathbf{E}_{st3}$  respectively, i.e.,

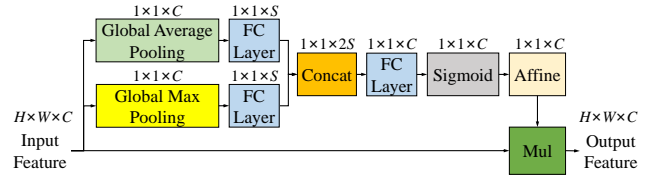


Figure 2: Schema of Channel-wise DNA module (cDNA).

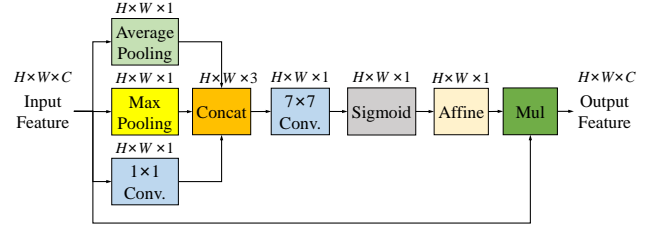


Figure 3: Schema of Spatial DNA module (sDNA).

$$\mathbf{E}_{st1} = \text{Conv}^{1 \times 1}(\mathbf{F}_{st}), \quad (9)$$

$$\mathbf{E}_{st2} = \text{MaxPool}(\mathbf{F}_{st}), \quad (10)$$

$$\mathbf{E}_{st3} = \text{AvgPool}(\mathbf{F}_{st}). \quad (11)$$

These three spatial features are then concatenated and forwarded to  $7 \times 7$  convolution layer to encode contextual information into local features. After Sigmoid activation, we apply affine transformation with weight  $\omega_{st}$  and bias  $b_{st}$  to rescale normalized attentions. Finally, we multiply attention map  $\mathbf{W}_{st}'$  with input feature map  $\mathbf{F}_{st}$ . In short, the spatial attention is computed as:

$$\mathbf{E}_{st} = \text{Concat}(\mathbf{E}_{st1}, \mathbf{E}_{st2}, \mathbf{E}_{st3}), \quad (12)$$

$$\mathbf{W}_{st}' = \omega_{st}(\text{Sigmoid}(\mathbf{E}_{st})) + b_{st}, \quad (13)$$

$$\mathbf{F}_{st}' = \mathbf{W}_{st}' \otimes \mathbf{F}_{st}, \quad (14)$$

where  $\otimes$  denotes element-wise multiplication, and  $\mathbf{F}_{st}'$  is feature map enhanced by our sDNA module. Our sDNA and cDNA modules are both integrated into residual units of HRNet for feature enhancement, as is show in Figure 4. There are two different sequential orders for spatial and channel attentions: cDNA-first arrangement and sDNA-first arrangement. The choice of sequential arrangements for DNAs will be discussed by ablation studies in Section 4.

### 3.2.3 rDNA: Resolution-wise De-Normalized Attention

The importance of features from different resolutions changes under diverse contexts. Low-resolution features with large receptive fields help invisible keypoint inference, while high-resolution features provide pixel-level details for accurate keypoint estimation. Therefore, we propose to evaluate importance of features from different resolutions to improve the information fusion method of HRNet. As is mentioned in Section 3.1, the outputs of feature fusion modules in original HRNet are computed as:

$$\mathbf{Y}_i = \sum_{i=1}^M \text{T}(\mathbf{X}_h, i), \quad (15)$$

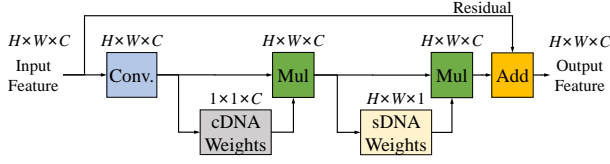


Figure 4: Integrating cDNA and sDNA modules into residual unit.

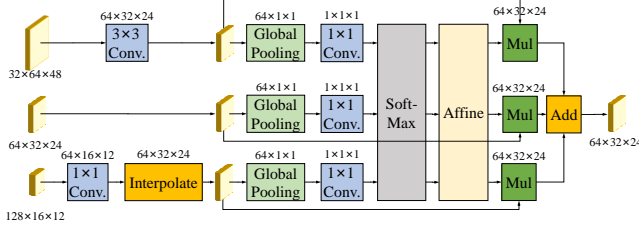


Figure 5: An example of Resolution-wise DNA module (rDNA). Features from three resolutions are aggregated in this module.

Instead of directly adding rescaled feature maps as Equation (15), we propose to replace feature fusion module in HRNet with Resolution-wise De-Normalized Attention (rDNA) module, which learns a group of nonlinear scalars  $\mathbf{W}_{res}^h = \{W_{res}^1, W_{res}^2, \dots, W_{res}^M\}$  as attention weights to improve feature aggregation between parallel subnets, i.e.,

$$\mathbf{Y}_i = \sum_{h=1}^M W_{res}^h T(\mathbf{X}_h, i), \quad (16)$$

where  $\mathbf{X} = \{\mathbf{X}_1, \mathbf{X}_2, \dots, \mathbf{X}_M\}$  and  $\mathbf{Y} = \{\mathbf{Y}_1, \mathbf{Y}_2, \dots, \mathbf{Y}_M\}$  are input and output features of  $M$  resolutions, and  $h \in \{1, 2, \dots, M\}$  denotes the index of input features. To obtain our rDNA attention map, we firstly transform features of different scales to the same resolution  $r$  with sampling function  $T$ , and then we aggregate each feature map with global pooling and  $1 \times 1$  convolution functions, i.e.,

$$\mathbf{X}_h' = T(\mathbf{X}_h, r), \quad (17)$$

$$E_h = \text{Conv}^{1 \times 1}(\text{GlobalPool}(\mathbf{X}_h')), \quad (18)$$

where  $\mathbf{X}_h'$  is rescaled feature map of resolution  $h$ , and  $E_h$  is a scalar with contextual information of the  $h$ th resolution.

After feature aggregation, we activate our attention weights with de-normalized SoftMax function to get non-linearity and avoid feature attenuation. The rDNA weights  $\mathbf{W}_{res}^h$  are finally calculated by:

$$W_{res}^h = e^{E_h} / (\sum_{i=1}^M e^{E_i}), \quad (19)$$

$$W_{res}^h = \omega_{res}(W_{res}^h) + b_{res}, \quad (20)$$

where  $\omega_{res}$  and  $b_{res}$  are respectively weight and bias for affine transformation, and  $W_{res}^h$  is a scalar that represents the importance of features from the  $h$ th resolution. Figure 5 displays an example of our proposed rDNA module, in which features from three resolutions are aggregated.

### 3.3 Modifications on HRNet Architecture

#### 3.3.1 Going Deeper with HRNet

The main body of HRNet is composed of parallel multi-resolution subnetworks with repeated information fusion between stages. An example HRNet with 4 parallel subnetworks is given in Equation (1). To establish information exchange across resolutions inside HRNet layers, we add fine-to-coarse connections across different resolutions in each layer of HRNet, which extends the longest path of network topology and enhances the capability for feature representations. Following the example in Equation (1), our fine-to-coarse connections are illustrated as follows:

$$\begin{aligned} N_{22} &\rightarrow N_{21} \\ N_{33} &\rightarrow N_{32} \rightarrow N_{31} \\ N_{44} &\rightarrow N_{43} \rightarrow N_{42} \rightarrow N_{41}, \end{aligned} \quad (21)$$

where  $s$  is stage index and  $r$  is resolution index, and  $N_{sr}$  denotes subnetwork in the  $s$ th stage and the  $r$ th resolution. The comparison between main bodies of original HRNet and our modified network is shown in Figure 1, in which red arrows denote the longest paths of network topologies.

Our modified HRNet with fine-to coarse connections can also be displayed as Figure 6 when we arrange our network topology along the longest path, which looks like a Stacked Hourglass Network (Newell, Yang, and Deng 2016) with skip connections. The performance of our fine-to-coarse connections will be demonstrated by experiments in Section 4.

#### 3.3.2 Modification on Heatmap Regression

We propose to modify the heatmap regressor at the end of HRNet for efficient feature combination and precise key-point prediction, which is similar to RefineNet (Lin et al. 2017). We adopt a hierarchical method to regress heatmaps by gradually merging features from low to high resolutions, as is shown in Figure 7. Given encoded feature maps  $\mathbf{X} = \{\mathbf{X}_1, \mathbf{X}_2, \dots, \mathbf{X}_M\}$  of  $M$  resolutions, the feature of the  $r$ th resolution ( $r > 1$ ) is upsampled by interpolation (denoted as Int) and deconvolution (denoted as Deconv) operations respectively. The two upsampled feature maps are added and concatenated with feature from the  $(r - 1)$ th resolution. The feature maps are progressively updated from low to high resolutions as Equation (22) and Equation (23), and we finally regress updated feature of the highest resolution with convolution to predict the heatmap  $\mathbf{H}$ , i.e.,

$$\mathbf{X}_{r-1}' = \text{Int}(\mathbf{X}_r) + \text{Deconv}(\mathbf{X}_r), \quad (22)$$

$$\mathbf{X}_{r-1} = \text{Concat}(\mathbf{X}_{r-1}', \mathbf{X}_{r-1}). \quad (23)$$

$$\mathbf{H} = \text{Conv}(\mathbf{X}_1). \quad (24)$$

Mean squared error (MSE) is applied as loss function of our heatmap regressor. We'll demonstrate the effectiveness of our proposed heatmap regressor in Section 4.

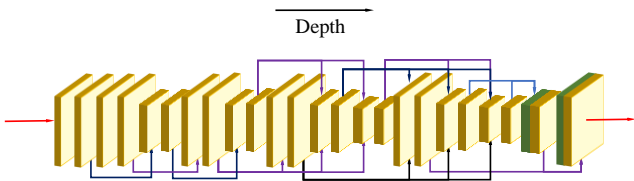


Figure 6: Arranging the topology of our network along the depth.

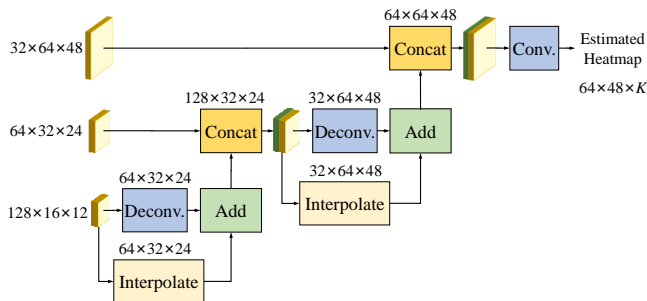


Figure 7: Modified keypoint regression module, which regresses heatmaps by merging features from low to high resolutions.

## 4. Experiments

### 4.1 Experimental Setup

**Dataset and Metric.** We demonstrate the effectiveness of our methods on COCO keypoint benchmark (Lin et al. 2014). The COCO dataset contains more than 200k images and 250k person instances. Our networks are only trained on COCO train2017 set, and evaluated on COCO val2017 set for comparison with public state-of-the-art methods. We use OKS-based mean average precision (Lin et al. 2014) as evaluation metric on COCO dataset, where OKS (object keypoint similarity) is calculated from similarity between predicted keypoints and ground truth positions.

**Training.** The human detection box of our network is made to a fixed aspect ratio, i.e.,  $height:weight = 4:3$  for COCO dataset. Following state-of-the-art method (Sun et al. 2019) for fair comparison, our data augmentation includes random scaling ( $[-35\%, 35\%]$ ), random rotation ( $[-45^\circ, 45^\circ]$ ) and flipping. We employ SGDR (Loshchilov and Hutter 2017) as optimizer with initial learning rate of 0.001,  $T_0 = 1$ , and  $T_{mul} = 2$ . Our networks are trained for 255 epochs with batch size 64 on 8 TITAN V GPUs.

**Testing.** For COCO benchmark, a two-stage top-down paradigm is used, which firstly detects persons and then estimates keypoints of detected human bodies. We use the same faster-RCNN (Ren et al. 2015) human detector as SimpleBaseline (Xiao, Wu, and Wei 2018) with 56.4 AP. Following the common practice (Newell, Yang, and Deng 2016; Chen et al. 2018), the keypoints are predicted by averaging heatmaps of original and flipped images. A quarter offset from the highest response to the second highest response is used to predict the final keypoints.

Description	Param.	FLOPs	AP
Original HRNet W32	28.5M	7.10G	74.46
HRNet W32 + channel-wise attention	28.5M	7.12G	74.8
HRNet W32 + cDNA	28.5M	7.12G	75.0
HRNet W32 + spatial attention	28.5M	7.12G	74.6
HRNet W32 + sDNA	28.5M	7.12G	74.8
HRNet W32 + resolution-wise attention	28.5M	7.12G	74.4
HRNet W32 + rDNA	28.6M	7.12G	74.9
HRNet W32 + cDNA + sDNA	28.6M	7.13G	<b>75.1</b>
HRNet W32 + sDNA + cDNA	28.6M	7.13G	74.7
HRNet W32 + cDNA + sDNA + rDNA	28.6M	7.13G	<b>75.4</b>
HRNet W32 + f2c	29.5M	7.26G	74.9
HRNet W32 + modified regressor	30.4M	7.51G	75.1
HRNet W32 + f2c + modified regressor	31.4M	7.63G	<b>75.3</b>
HRNet W32 + all proposed modules	31.5M	7.66G	<b>76.1</b>

Table 1: Results of component ablation studies. We firstly demonstrate the performance of three types of DNA modules and discuss the sequential arrangement of cDNA and sDNA modules. Then we illustrate the effectiveness of our modifications on HRNet architecture. We finally show the performance with all proposed modules integrated into HRNet.

### 4.2 Component Ablation Studies

In this subsection, we demonstrate the effectiveness of our proposed modules on COCO val2017 dataset, the results are displayed in Table 1. We use HRNet W32 as backbone and input size of  $256 \times 192$  in all ablation studies.

**Effectiveness of DNAs.** We show the performance of three types of DNA modules experimentally on COCO benchmark (Lin et al. 2014). To illustrate the effectiveness of de-normalizing operations, we firstly demonstrate the performance of three conventional attentions (channel-wise attention, spatial attention, and resolution-wise attention), which is compared with three DNA modules (cDNA, sDNA, rDNA) respectively. As is shown in top of Table 1, DNA-based modules outperform other three mentioned attention modules with similar functions.

**Arrangement of DNAs.** The rDNA modules can only be integrated between parallel subnetworks, so there is no need for discussion. However, for the other two DNAs, there are two different sequential arrangements for cDNA and sDNA: cDNA-first and sDNA-first arrangements. As is shown in the middle of Table 1, sDNA-first arrangement performs worse than sDNA or cDNA alone, while cDNA-first arrangement provides better performance. Our result is contrary to the conclusion of SCARB (Su et al. 2019), which may be due to our different attention structures.

**Modifications on Architecture.** We also illustrate the effectiveness of our proposed fine-to-coarse connections (abbreviated as f2c) and keypoint heatmap regressor, as is shown at the bottom of Table 1. We also integrate all our proposed modules into HRNet, and have achieved state-of-the-art performance on human pose estimation.

Approach	Backbone	Input size	Param.	FLOPs	AP
Hourglass	Hourglass	256×192	25.1M	14.3G	66.9
CPN	ResNet 50	256×192	27.0M	6.2G	68.6
CPN + OHKM	ResNet 50	256×192	27.0M	6.2G	69.4
SimpleBaseline	ResNet 152	256×192	68.6M	15.7G	72.1
HRNet W32	HRNet W32	256×192	28.5M	7.1G	74.5
HRNet W48	HRNet W48	256×192	63.6M	14.6G	75.1
DNANet W32 (Ours)	DNANet W32	256×192	31.5M	7.7G	<b>76.1</b>
DNANet W48 (Ours)	DNANet W48	256×192	70.3M	15.8G	<b>76.5</b>
SimpleBaseline	ResNet 152	384×288	68.6M	35.6G	74.3
HRNet W32	HRNet W32	384×288	28.5M	16.0G	75.8
HRNet W48	HRNet W48	384×288	63.6M	32.9G	76.3
DNANet W32 (Ours)	DNANet W32	384×288	31.5M	17.4G	<b>77.5</b>
DNANet W48 (Ours)	DNANet W48	384×288	70.3M	35.7G	<b>77.9</b>

Table 2: Comparing the performance of DNANet with other state-of-the-art methods on COCO val2017 dataset.

Approach	Backbone	Input size	Param.	FLOPs	AP
CPN	ResNet 50	384×288	-	-	72.1
Ensembled CPN	ResNet 50	384×288	-	-	73.0
SimpleBaseline	ResNet 152	384×288	68.6M	35.6G	73.7
HRNet W32	HRNet W32	384×288	28.5M	16.0G	74.9
HRNet W48	HRNet W48	384×288	63.6M	32.9G	75.5
DNANet W32 (Ours)	DNANet W32	384×288	31.5M	17.4G	<b>76.6</b>
DNANet W48 (Ours)	DNANet W48	384×288	70.3M	35.7G	<b>77.0</b>

Table 3: Comparing the performance of DNANet with other state-of-the-art methods on COCO test-dev2017 dataset.

### 4.3 Comparisons with SOTA Methods

In this subsection, we compare the performance of our proposed DNANet with other state-of-the-art (abbreviated as SOTA above) approaches, i.e., Stacked Hourglass Network (Newell, Yang, and Deng 2016), CPN (Chen et al. 2018), SimpleBaseline (Xiao, Wu, and Wei 2018), and HRNet (Sun et al. 2019) respectively.

Due to limited pages, we only demonstrate the average precision on COCO val2017 dataset on Table 2 and test-dev2017 dataset on Table3. Our small network of width 32 (DNANet W32) performs even better than HRNet W48, which is useful for real-time applications. Our largest DNANet W48 with input size of 384×288 achieves 77.9 AP score on COCO val2017 set and 77.0 AP score on COCO test-dev 2017 dataset without using extra keypoint training dataset, which outperforms all other mentioned methods.

Our accuracy improvements on large networks (e.g., networks of W48) are less than light networks (e.g., networks of W32), which may due to that large networks are initially with saturated feature representation capabilities, so that attention modules cannot bring more performance increments to large networks.

## 5. Conclusion

In this paper, we introduce a new type of attention modules, namely De-Normalized Attentions (DNAs), which applies affine transformations to deal with attenuation in attention modules. Also, we extend HRNet with three DNAs to evaluate feature importance across spatial, channel-wise, and resolution-wise aspects. Furthermore, we modify the architecture of HRNet in two ways: we add fine-to-coarse connections in each layer of HRNet to lengthen the longest path of network topology, and we alter heatmap regression approach at the end of HRNet with deconvolutions, skip connections, and concatenations. Ablation studies show the effectiveness of our proposed methods, and we have achieved state-of-the-art performance at 76.9 AP score on COCO val2017 dataset without using any extra keypoint training data. For future work, our proposed DNANet can also be expanded on other pixel-labeling tasks, such as semantic segmentation and facial landmark detection.

## References

- Andriluka, M.; Pishchulin, L.; Gehler, P. V.; and Schiele, B. 2014. 2d human pose estimation: New benchmark and state of the art analysis. In *CVPR*.
- Badrinarayanan, V.; Kendall, A.; and Cipolla, R. 2017. Segnet: A deep convolutional encoder-decoder architecture for image segmentation. *IEEE Trans. Pattern Anal. Mach. Intell.*
- Bahdanau, D.; Cho, K.; and Bengio, Y. 2015. Neural machine translation by jointly learning to align and translate. In *ICLR*.
- Carreira, J.; Agrawal, P.; Fragkiadaki, K.; and Malik, J. 2016. Human pose estimation with iterative error feedback. In *CVPR*.
- Chen, Y.; Wang, Z.; Peng, Y.; Zhang, Z.; Yu, G.; and Sun, J. 2018. Cascaded pyramid network for multi-person pose estimation. In *CVPR*.
- Chen, Z.; Cui, Y.; Ma, W.; Wang, S.; and Hu, G. 2019. Convolutional spatial attention model for reading comprehension with multiple-choice questions. In *AAAI*.
- Cui, Y.; Liu, T.; Chen, Z.; Wang, S.; and Hu, G. 2016. Consensus attention-based neural networks for Chinese reading comprehension. In *COLING*.
- Dantone, M.; Gall, J.; Leistner, C.; and Gool, L. V. 2013. Human pose estimation using body parts dependent joint regressors. In *CVPR*.
- Dong, J.; Chen, Q.; Shen, X.; Yang, J.; and Yan, S. 2014. Towards unified human parsing and pose estimation. In *CVPR*.
- Dong, L.; Wang, B.; Zhao, M.; and Xu, W. 2017. Robust infrared maritime target detection based on visual attention and spatio-temporal filtering. *IEEE Trans. Geoscience and Remote Sensing*.
- Duan, X.; Yin, M.; Zhang, M.; Chen, B.; and Luo, W. 2019. Zero-shot cross-lingual abstractive sentence summarization through teaching generation and attention. In *ACL*.
- Fourure, D.; Emonet, R.; Fromont, É.; Muselet, D.; Trémeau, A.; and Wolf, C. 2017. Residual conv-deconv grid network for semantic segmentation. In *BMVC*.

- Fu, J.; Liu, J.; Tian, H.; Li, Y.; Bao, Y.; Fang, Z.; and Lu, H. 2019. Dual attention network for scene segmentation. In *CVPR*.
- Fu, L.; Zhang, J.; and Huang, K. 2015. Beyond tree structure models: A new occlusion aware graphical model for human pose estimation. In *ICCV*.
- Hara, K., and Chellappa, R. 2013. Computationally efficient regression on a dependency graph for human pose estimation. In *CVPR*.
- He, K.; Zhang, X.; Ren, S.; and Sun, J. 2016. Deep residual learning for image recognition. In *CVPR*.
- Hu, J.; Shen, L.; and Sun, G. 2018. Squeeze-and-excitation networks. In *CVPR*.
- Insafutdinov, E.; Andriluka, M.; Pishchulin, L.; Tang, S.; Levinkov, E.; Andres, B.; and Schiele, B. 2017. Arttrack: Articulated multi-person tracking in the wild. In *CVPR*.
- Iqbal, U.; Milan, A.; and Gall, J. 2017. Posetrack: Joint multi-person pose estimation and tracking. In *CVPR*.
- Kar, A.; Rai, N.; Sikka, K.; and Sharma, G. 2017. Adascan: Adaptive scan pooling in deep convolutional neural networks for human action recognition in videos. In *CVPR*.
- Ke, L.; Chang, M.; Qi, H.; and Lyu, S. 2018. Multiscale structure-aware network for human pose estimation. In *ECCV*.
- Kiefel, M., and Gehler, P. V. 2014. Human pose estimation with fields of parts. In *ECCV*.
- Li, H.; Xiong, P.; An, J.; and Wang, L. 2018. Pyramid attention network for semantic segmentation. In *BMVC*.
- Li, X.; Hu, X.; and Yang, J. 2019. Spatial group-wise enhance: Improving semantic feature learning in convolutional networks. *CoRR* abs/1905.09646.
- Liang, X.; Gong, K.; Shen, X.; and Lin, L. 2019. Look into person: Joint body parsing & pose estimation network and a new benchmark. *IEEE Trans. Pattern Anal. Mach. Intell.*
- Lin, T.; Maire, M.; Belongie, S. J.; Hays, J.; Perona, P.; Ramanan, D.; Dollár, P.; and Zitnick, C. L. 2014. Microsoft COCO: common objects in context. In *ECCV*.
- Lin, G.; Milan, A.; Shen, C.; and Reid, I. D. 2017. Refinenet: Multi-path refinement networks for high-resolution semantic segmentation. In *CVPR*.
- Loshchilov, I., and Hutter, F. 2017. SGDR: stochastic gradient descent with warm restarts. In *ICLR*.
- Lv, J.; Shao, X.; Xing, J.; Cheng, C.; and Zhou, X. 2017. A deep regression architecture with two-stage re-initialization for high performance facial landmark detection. In *CVPR*.
- Ma, S.; Fu, J.; Chen, C. W.; and Mei, T. 2018. DA-GAN: instance-level image translation by deep attention generative adversarial networks. In *CVPR*.
- Mejjati, Y. A.; Richardt, C.; Tompkin, J.; Cosker, D.; and Kim, K. I. 2018. Unsupervised attention-guided image-to-image translation. In *NeurIPS*.
- Mnih, V.; Heess, N.; Graves, A.; and Kavukcuoglu, K. 2014. Recurrent models of visual attention. In *NIPS*.
- Newell, A.; Yang, K.; and Deng, J. 2016. Stacked hourglass networks for human pose estimation. In *ECCV*.
- Nie, X.; Feng, J.; Zuo, Y.; and Yan, S. 2018. Human pose estimation with parsing induced learner. In *CVPR*.
- Noh, H.; Hong, S.; and Han, B. 2015. Learning deconvolution network for semantic segmentation. In *ICCV*.
- Ren, S.; He, K.; Girshick, R. B.; and Sun, J. 2015. Faster R-CNN: towards real-time object detection with region proposal networks. In *NIPS*.
- Ronneberger, O.; Fischer, P.; and Brox, T. 2015. U-net: Convolutional networks for biomedical image segmentation. In *MICCAI*.
- Rush, A. M.; Chopra, S.; and Weston, J. 2015. A neural attention model for abstractive sentence summarization. In *EMNLP*.
- Saxena, S., and Verbeek, J. 2016. Convolutional neural fabrics. In *NIPS*.
- Shen, T.; Zhou, T.; Long, G.; Jiang, J.; Pan, S.; and Zhang, C. 2018. Disan: Directional self-attention network for rnn/cnn-free language understanding. In *AAAI*.
- Simonyan, K., and Zisserman, A. 2015. Very deep convolutional networks for large-scale image recognition. In *ICLR*.
- Su, K.; Yu, D.; Xu, Z.; Geng, X.; and Wang, C. 2019. Multi-person pose estimation with enhanced channel-wise and spatial information. *CoRR* abs/1905.03466.
- Sun, K.; Xiao, B.; Liu, D.; and Wang, J. 2019. Deep high-resolution representation learning for human pose estimation. *CoRR* abs/1902.09212.
- Sun, M.; Kohli, P.; and Shotton, J. 2012. Conditional regression forests for human pose estimation. In *CVPR*.
- Tan, M., and Le, Q. V. 2019. Efficientnet: Rethinking model scaling for convolutional neural networks. In *ICML*.
- Toshev, A., and Szegedy, C. 2014. Deeppose: Human pose estimation via deep neural networks. In *CVPR*.
- Vaswani, A.; Shazeer, N.; Parmar, N.; Uszkoreit, J.; Jones, L.; Gomez, A. N.; Kaiser, L.; and Polosukhin, I. 2017. Attention is all you need. In *NIPS*.
- Wang, Y., and Mori, G. 2008. Multiple tree models for occlusion and spatial constraints in human pose estimation. In *ECCV*.
- Wang, F.; Jiang, M.; Qian, C.; Yang, S.; Li, C.; Zhang, H.; Wang, X.; and Tang, X. 2017. Residual attention network for image classification. In *CVPR*.
- Wei, S.; Ramakrishna, V.; Kanade, T.; and Sheikh, Y. 2016. Convolutional pose machines. In *CVPR*.
- Woo, S.; Park, J.; Lee, J.; and Kweon, I. S. 2018. CBAM: convolutional block attention module. In *ECCV*.
- Xiao, S.; Feng, J.; Xing, J.; Lai, H.; Yan, S.; and Kassim, A. A. 2016. Robust facial landmark detection via recurrent attentive-refinement networks. In *ECCV*.
- Xiao, B.; Wu, H.; and Wei, Y. 2018. Simple baselines for human pose estimation and tracking. In *ECCV*.
- Xiu, Y.; Li, J.; Wang, H.; Fang, Y.; and Lu, C. 2018. Pose flow: Efficient online pose tracking. In *BMVC*.
- Xu, C.; Hsieh, S.; Xiong, C.; and Corso, J. J. 2015. Can humans fly? action understanding with multiple classes of actors. In *CVPR*.
- Xu, G.; Xu, L.; Lv, C.; and Zhu, B. 2017. An improved head pose estimation method for the robotic wheelchair interaction control. In *ROBIO*.
- Yan, S.; Xiong, Y.; and Lin, D. 2018. Spatial temporal graph convolutional networks for skeleton-based action recognition. In *AAAI*.
- Yang, W.; Li, S.; Ouyang, W.; Li, H.; and Wang, X. 2017. Learning feature pyramids for human pose estimation. In *ICCV*.

- Yu, C.; Wang, J.; Peng, C.; Gao, C.; Yu, G.; and Sang, N. 2018. Bisenet: Bilateral segmentation network for real-time semantic segmentation. In *ECCV*.
- Zhang, D.; Guo, G.; Huang, D.; and Han, J. 2018. Poseflow: A deep motion representation for understanding human behaviors in videos. In *CVPR*.
- Zhang, H.; Goodfellow, I. J.; Metaxas, D. N.; and Odena, A. 2019. Self-attention generative adversarial networks. In *ICML*.
- Zhou, Y.; Sun, X.; Zha, Z.; and Zeng, W. 2018. Mict: Mixed 3d/2d convolutional tube for human action recognition. In *CVPR*.
- Zhou, Y.; Hu, X.; and Zhang, B. 2015. Interlinked convolutional neural networks for face parsing. In *ISNN*.
- Zhu, Y.; Zhao, C.; Guo, H.; Wang, J.; Zhao, X.; and Lu, H. 2019. Attention couplenet: Fully convolutional attention coupling network for object detection. *IEEE Trans. Image Processing*.